ADVANCED OPTICAL MATERIALS
www.advopticalmat.de

A Tunable Metasurface with Switchable Functionalities: From Perfect Transparency to Perfect Absorption

Yue Li, Jing Lin, Huijie Guo, Wujiong Sun, Shiyi Xiao, and Lei Zhou**

A thin screen exhibiting dynamically switchable transmission/absorption functionalities is highly desired in practice. However, a trilayer transmissive metasurface with active elements controlled in a uniform manner cannot exhibit independently controlled transmission and absorption properties due to intriguing interplays between the scattering and absorbing properties in systems exhibiting inversion symmetries. This motivates to employ the coupled-mode theory to establish a generic phase diagram for such transmissive metasurfaces with active elements loaded in different layers tuned independently and to guide researchers design tunable metadevices with completely decoupled transmission/absorption responses. Based on such a phase diagram, a microwave metasurface is designed/fabricated with PIN diodes incorporated, and it is experimentally demonstrated that its functionality can switch from perfect transparency to perfect absorption, controlled by external voltages applied across the diodes. In addition to finding immediate applications in practice (e.g., smart radomes), the results of this study also provide a new type of tunable meta-atom for building metasurfaces with flexible wave-front control abilities.

1. Introduction

Manipulating electromagnetic (EM) waves in predesigned manners are of great importance, due to many different application requests in practice. For example, a thin screen that allows perfect transmission of EM waves within a certain frequency interval is highly desired in applications related to EM-wave filters and radar radomes,[1] while a thin film that absorbs EM energy with 100% efficiency can be very useful in energy harvesting and invisibility-related applications.[2–4] Moreover, it is even more fascinating if one can combine those two functionalities into one single device, which can behave either as an ideal filter (as shown in **Figure 1**a) or a perfect absorber (as shown in Figure 1b), controlled dynamically by certain external knobs. Such tunable devices can be potentially useful in many application scenarios (e.g., smart radar radomes and solar cells), but are extremely challenging to realize since the two EM-wave properties (i.e., scattering and absorption) of an ultrathin slab are strongly coupled with each other. In fact, early theoretical studies have demonstrated that the largest absorption enabled by an ultrathin screen is 50% (as shown in Figure 1c,d),[5] not mentioning further difficulties in making the device actively tunable.

Recent developments on metasurface (particularly on tunable metasurfaces) provide possible solutions to make such optical devices. Metasurfaces,[6–12] ultrathin metamaterials composed by planar meta-atoms with tailored EM properties, have exhibited strong abilities to control EM waves,[6,7,13–16] with perfect transmission[17] and absorption[18] of EM waves both realized. With active elements integrated, one can further construct tunable metasurfaces with dynamically controlled functionalities[19–29] including tunable absorbers and filters. However, most tunable metadevices realized so far are based on reflection geometry[20–23,26–29] which are relatively easy to design, since only two channels exist in such systems for EM waves to radiate or dissipate (i.e., the reflection port and absorption).[30] In contrast, high-performance tunable metadevices in transmission modes are rarely seen, not mentioning those exhibiting dynamically switched dual functionalities. The intrinsic physics is that a transmissive metasurface has three channels (i.e., transmission and reflection ports, and absorption) to transport/dissipate energy, which must be carefully balanced to yield the desired functionalities (i.e., perfect transmission or perfect absorption). However, the competitions between these three channels are very complicated, which make a transmission-absorption switchable metadevice very difficult to realize, especially on an ultrathin platform.

In this paper, we design and experimentally realize such a metadevice with ultrathin thickness. In Section 2, we start from examining the EM properties a trilayer metasurface with PIN diodes loaded and controlled by the same voltages, and show that such a device cannot exhibit freely controlled transmission and absorption properties. We next employ the coupled-mode

Y. Li, Prof. S. Xiao
Key laboratory of Specialty Fiber Optics and Optical Access Networks
Joint International Research Laboratory of Specialty Fiber Optics and Advanced Communication
Shanghai Institute for Advanced Communication and Data Science
Shanghai University
Shanghai 200444, China
E-mail: phxiao@shu.edu.cn

J. Lin, H. Guo, Dr. W. Sun, Prof. L. Zhou
State Key Laboratory of Surface Physics and Department of Physics
Fudan University
Shanghai 200433, China
E-mail: phzhou@fudan.edu.cn

The ORCID identification number(s) for the author(s) of this article can be found under https://doi.org/10.1002/adom.201901548.

DOI: 10.1002/adom.201901548

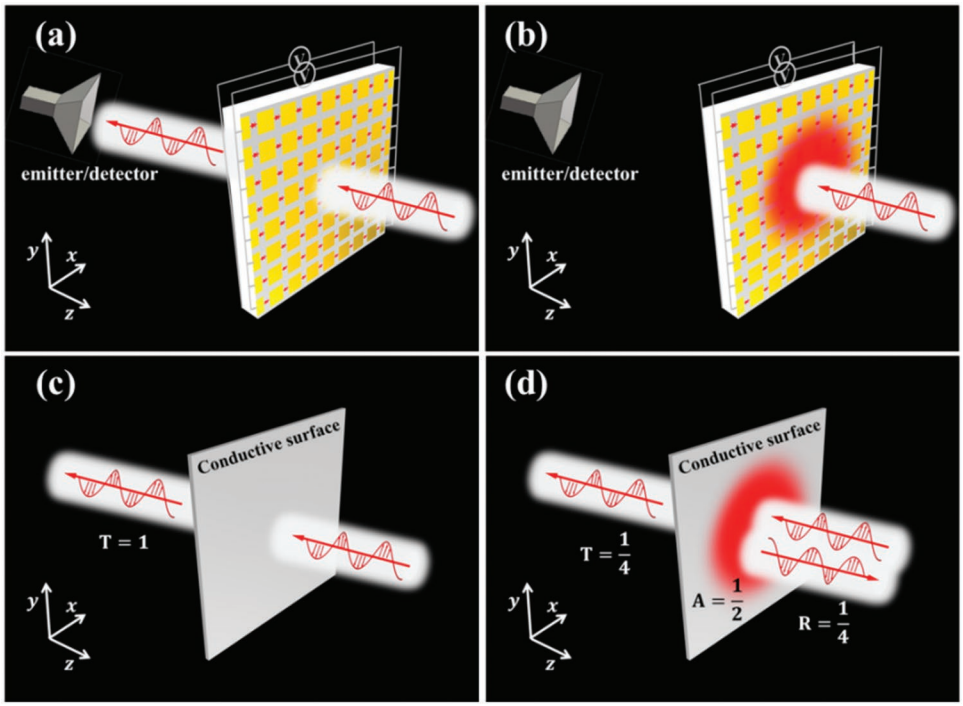

Figure 1. Schematics and working principles of the active optical transparent window. a) ON-state is an ideal filter and b) OFF-state is a perfect absorber. c,d) Working status of conductive surface with $\sigma = 0$ (perfect transparent) and $\sigma = 2/(Z_0 h)$ (maximum absorption $A = 50\%$.). Z_0 is the vacuum impedance and h is thickness of conductive surface in free space (see Section SI in the Supporting Information).

theory (CMT)[31–34] to reveal that such issue is caused by the intrinsic correlations between transmission and absorption properties of ultrathin systems with inversion symmetries (Section 3). We further employ the CMT (Section 4) to establish a generic phase diagram for such trilayer metasurfaces with upper and bottom layers controlled in different manners, and reveal the critical role of such actively inserted asymmetry to decouple these two strongly connected properties. As a proof of concept, we finally design and fabricate a tunable microwave metasurface based on the generic phase diagram, and experimentally demonstrate that it exhibits the desired dual functionalities, dynamically controlled by appropriate voltages applied across the PIN diodes incorporated. Our results not only provide new solutions to dynamically control the transmission and absorption of EM waves which may find many applications in practice, but also offer a new type of active meta-atom for building transmissive metasurfaces to dynamically manipulate EM wave fronts.

2. Experimental Characterizations on a Symmetric Metasurface

As schematically shown in **Figure 2**a, we start from examining the EM properties of a trilayer metasurface with active elements incorporated and controlled in the same way. We choose such ABA geometry to build our passive metasurface since such structure is proven to allow perfect transmission of EM waves within a certain frequency interval under appropriate conditions.[1] Specifically, the passive metasurface consists of a metallic mesh layer (B layer) sandwiched by two layers of metallic patches (A layer). To make the metasurface actively tunable, we insert PIN diodes (SMP1321-079) into those gaps between two metallic patches on two A layers. As shown in Figure 2a, we apply the same bias voltage (V_g) across each PIN diode, which can tune the dynamic resistance R_D (see inset to Figure 2b for equivalent circuit model of the PIN diode), and in turn, the EM properties of the patch resonators in two A layers. We fabricate a sample (see Figure 2b for its picture) and then experimentally characterize its EM properties as varying the bias voltage V_g. In our measurements, we illuminate the sample at a small incidence angle (≈ 5°) by a x-polarized plane wave emitted from a horn antenna, and then collect the reflected and transmitted signals by another horn antenna. Both source and detecting horn antennas are connected to a vector-field analyzer (Agilent E8362C).

Figure 2c–g depicts how the measured transmittance/reflectance spectra vary against the bias voltages applied. When the PIN diodes are unbiased (V_g = 0 V) indicating that each diode has a maximum resistance $R_D \approx 1 \times 10^6\ \Omega$, the metasurface exhibits a transparency window (5.8 − 7.4 GHz) with two perfect transmission peaks, caused by the resonance-induced transparency in ABA structures.[1] Meanwhile, the metasurface exhibits negligible absorption, as expected. As V_g increases, transmittance through our metasurface drops continuously with two peaks remaining at the same frequencies. At a threshold bias voltage ($V_s = 0.55$ V), the PIN diodes exhibit small-enough resistances ($R_D \approx 273\ \Omega$) to electrically connect two adjacent metallic patches, which completely eliminates the original resonances supported by two A layers. As a result, the transmittance spectrum of our metasurface stops showing

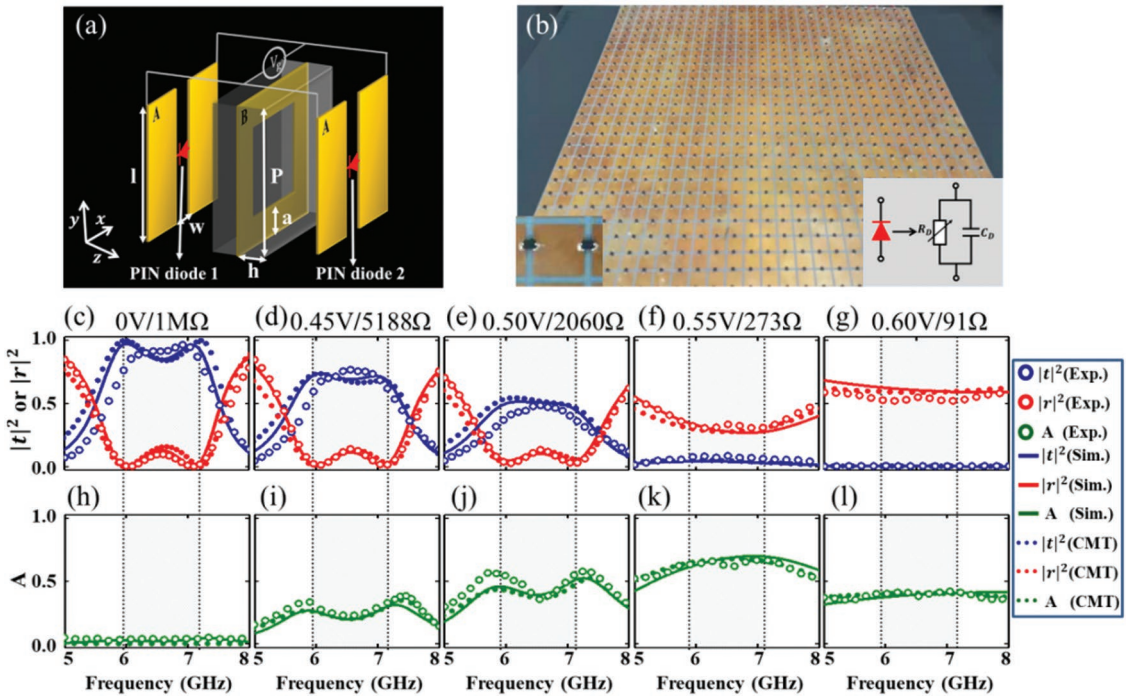

Figure 2. Sample design, fabrication, and experimental characterization. a) Scheme of the trilayer structure (metallic mesh layer (B layer) sandwiched by two layers of metallic patches (A layer)) with optimized geometric parameters of p = 8 mm, l = 6 mm, w = 1 mm, h = 1 mm, and a = 1.75 mm. b) The photograph of the fabricated sample. Inset shows the enlarged view of the unit cell and equivalent circuit of the PIN diode. c–l) The transmittance (blue), reflectance (red), and absorption (green) with different bias voltages or equivalent resistances of PIN diodes, obtained by experiment (symbols), FDTD simulation (curves), and CMT mode (short dot).

any transparency feature at $V_g > V_s$, simply because the resonances in A layers are killed by electric shorting. All experiment results are in excellent agreement with finite-difference-time-domain (FDTD) simulations on realistic systems, in which an equivalent circuit consisting of a capacitor (C_D) and a resistor (R_D) (see Figure 2b) is adopted model for the PIN diode. In our simulations, we set C_D as 0.15 pF according to ref. [35], and obtained the relation of $R_D \sim V_g$ directly from the experimental IV curves. (Experimental data in very good agreement with the Shockley equation, see Section SIV in the Supporting Information for details). Our experimental results clearly demonstrate that a full-range transmittance modulation can be achieved through tuning the bias voltage.

On the other side, the absorption spectrum of our metasurface exhibits a distinct V_g dependence compared to the transmittance spectrum. As illustrated in Figure 2h–l, as V_g increases from 0 to 0.55 V, a peak appears in the absorption spectrum (defined as $A = 1 - |t|^2 - |r|^2$) and its strength increases monotonically along with the decrement in transmission. However, as V_g further increases to exceed a critical value (0.55 V), the peak absorption value starts to drop in the same manner as the transmittance, indicating that such a system exhibits a maximum absorption ($A \approx 66\%$) at a critical bias voltage (V_g = 0.55 V). Compared with the single conductive sheet with maximum absorption A = 50%, our trilayer metasurface can achieve an enhanced maximum absorption, but the achieved value is still much less than 100%.[36] Obviously, as $V_g > 0.55$ V, the reflectance starts to increase dramatically, which explains why we cannot further enhance A through suppressing T.

3. CMT Analyses on Experimental Results

To understand the intriguing experimental results reported in last section, we employ a CMT model to analyze the EM properties of such tunable metasurfaces.[31–33] Noting that the metallic mesh can well block EM waves at frequencies below 25 GHz (the cutoff frequency of the mesh),[37] thus severing as an optically opaque background for the whole system, and the patches on two A layers provide two electric resonances, we can describe such a system as a two-port model with two resonators embedded inside an opaque background (see **Figure 3**a). Therefore, according to the CMT model,[32,33] we find that the time evolution of the amplitudes a_i (i = 1, 2) of two resonant modes (contributed by two A layers) are governed by the following equations

$$\frac{1}{2\pi}\frac{\mathrm{d}}{\mathrm{d}t}\begin{pmatrix} a_1 \\ a_2 \end{pmatrix} = \left[i\begin{pmatrix} f_1 & \kappa \\ \kappa & f_2 \end{pmatrix} + \begin{pmatrix} -\Gamma_1 & X \\ X & -\Gamma_2 \end{pmatrix} + \begin{pmatrix} -\Gamma_1^A & 0 \\ 0 & -\Gamma_2^A \end{pmatrix} \right] \begin{pmatrix} a_1 \\ a_2 \end{pmatrix} + \begin{pmatrix} d_{11} & d_{21} \\ d_{12} & d_{22} \end{pmatrix} \begin{pmatrix} S_1^{\mathrm{in}} \\ S_2^{\mathrm{in}} \end{pmatrix} \quad (1)$$

where f_1 and f_2 are the resonating frequencies of two modes, Γ_i and Γ_i^A are the radiation and absorptive decay rates of the ith mode (i = 1, 2), d_{ni} describes the coupling between the ith mode and the nth external port (n = 1, 2 stands for the reflection and transmission ports, respectively), κ denotes the near-field coupling between two "modes" through the evanescent-wave overlapping across the metallic mesh, and X denotes the interactions between two resonant modes at the far field. We note that X and Γ_i are not independent parameters, but

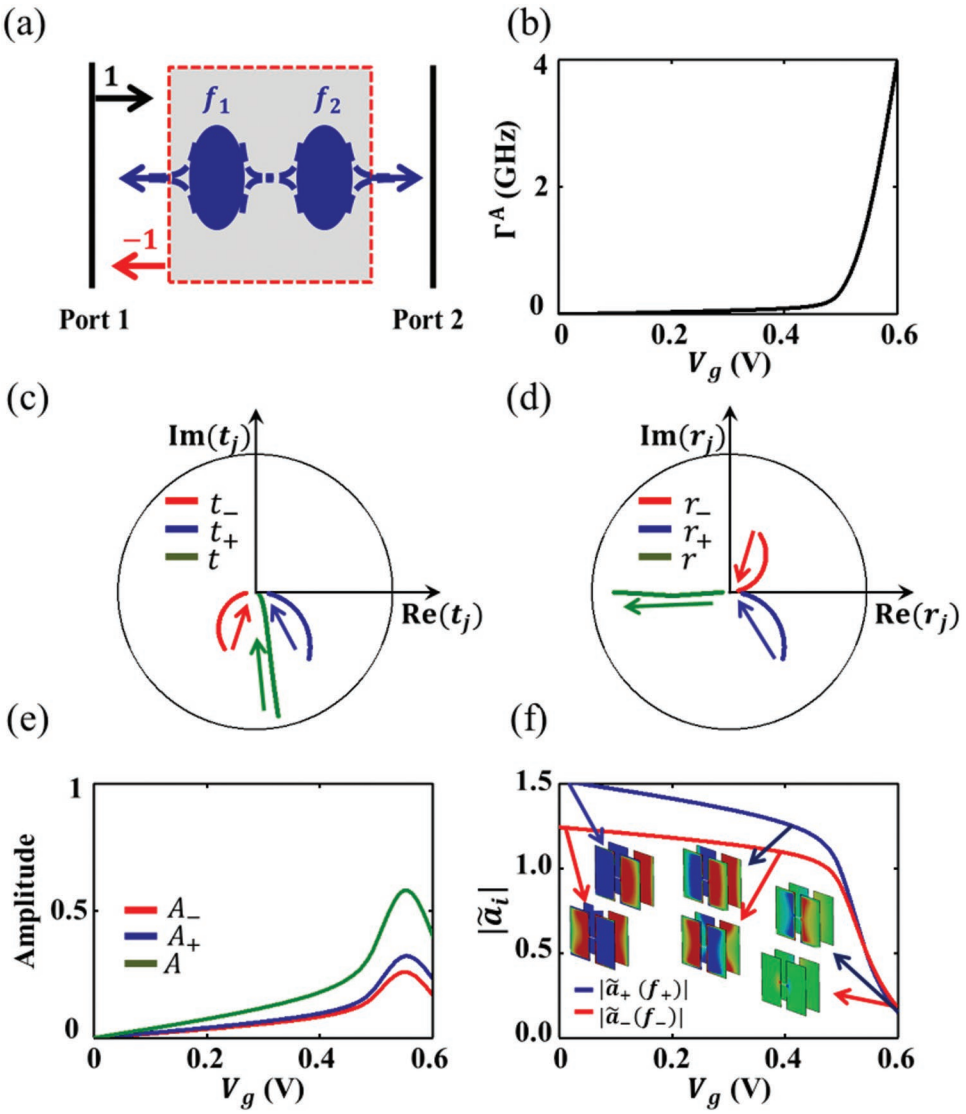

Figure 3. CMT model and theoretical analysis. a) Scheme of two resonators system coupled with two ports in opaque background. b) Retrieved relationship between absorptive decay rate (Γ^A) and gate voltage V_g. c) Transmission, d) reflection, and e) absorption of the symmetric mode and antisymmetric mode as a function of gate voltage V_g. f) Amplitude of symmetric and antisymmetric collective mode as a function of gate voltage V_g.

are correlated with each other via $X = -(d_{11}^* d_{12} + d_{21}^* d_{22})/2$ and $\Gamma_i = (|d_{1i}|^2 + |d_{2i}|^2)/2$.[32,33] Moreover, while Equation (1) applies to general two-mode systems without any restrictions, for the cases studied in last section, we have the following relations between different parameters: $f_1 = f_2$, $\Gamma_1 = \Gamma_2$, $\Gamma_1^A = \Gamma_2^A = \Gamma^A$. Therefore, we have totally four independent model parameters, which are f_1, Γ_1, Γ^A, and κ. Here, f_1, Γ_1, and κ are determined by the unbiased resonant structure (the original structure plus the PIN diodes but with inserted resistance set to infinity), while Γ^A (the absorption decay rate of the resonator) is mainly determined by the resistance of the PIN diode. The PIN diode we used contains a capacitor in parallel connection with a resistor whose resistance can be dynamically tuned by the bias voltage. Within the tuning range of the resistance (91 Ω to 1 MΩ), we can approximately treat the effect of the resistor as a perturbation to the whole system. Based on the perturbation theory,[38] we finally derived a semianalytical relation between Γ^A and R_D, showing that Γ^A is inversely proportional to R_D (see Section SIV in the Supporting Information for details). However, lacking analytical forms of other three parameters, here we chose to determine all four independent model parameters from fitting with FDTD results, for the sake of consistency.

We diagonalize the matrix (see Section SII in the Supporting Information) in Equation (1) containing the near-field coupling κ, and arrive at the following equation to determine the evolutions of amplitude $\tilde{a}_\pm$ (tilde (~) denotes CMT parameters for collective modes) of two resulting collective modes

$$\frac{1}{2\pi}\frac{\mathrm{d}}{\mathrm{d}t}\begin{pmatrix}\tilde{a}_-\\ \tilde{a}_+\end{pmatrix} = \left[i\begin{pmatrix}\tilde{f}_- & 0\\ 0 & \tilde{f}_+\end{pmatrix} + \begin{pmatrix}-\tilde{\Gamma}_-^S & 0\\ 0 & -\tilde{\Gamma}_+^S\end{pmatrix} + \begin{pmatrix}-\tilde{\Gamma}_-^A & 0\\ 0 & -\tilde{\Gamma}_+^A\end{pmatrix}\right]\begin{pmatrix}\tilde{a}_-\\ \tilde{a}_+\end{pmatrix} + \begin{pmatrix}\tilde{d}_{1-} & \tilde{d}_{2-}\\ \tilde{d}_{1+} & \tilde{d}_{2+}\end{pmatrix}\begin{pmatrix}S_1^{\mathrm{in}}\\ S_2^{\mathrm{in}}\end{pmatrix} \quad (2)$$

where $\tilde{f}_- = f_1 - \kappa$ and $\tilde{f}_+ = f_2 + \kappa$ are the eigenfrequencies of two collective modes with radiation decay rates given by

$\tilde{\Gamma}_-^S = \Gamma_1 + X$ and $\tilde{\Gamma}_+^S = \Gamma_2 - X$, $\tilde{\Gamma}_+^A = \tilde{\Gamma}_-^A = \Gamma^A$ are the absorptive decay rates, and subscript "+" denotes the symmetric mode ($\tilde{d}_{1+} = \tilde{d}_{2+}$) and "–" denotes antisymmetric mode ($\tilde{d}_{1-} = -\tilde{d}_{2-}$). Through standard CMT analyses, we find that the transmission coefficients and reflection coefficients are given by

$$t = \frac{\tilde{\Gamma}_+^S}{i\left(f - \tilde{f}_+\right) + \tilde{\Gamma}_+^S + \Gamma^A} - \frac{\tilde{\Gamma}_-^S}{i\left(f - \tilde{f}_-\right) + \tilde{\Gamma}_-^S + \Gamma^A} \tag{3}$$

$$r = -1 + \frac{\tilde{\Gamma}_+^S}{i\left(f - \tilde{f}_+\right) + \tilde{\Gamma}_+^S + \Gamma^A} + \frac{\tilde{\Gamma}_-^S}{i\left(f - \tilde{f}_-\right) + \tilde{\Gamma}_-^S + \Gamma^A} \tag{4}$$

Here, we have assumed for simplicity that the transmission through the background (i.e., the metallic mesh) is essentially 0, while the reflection from the background is –1, which is a reasonable assumption at frequencies far below the cutoff.

All experimental/numerical results depicted in Figure 2 can be well described by the CMT (i.e., Equations (3) and (4)) through carefully determining four fitting parameters (f_1, Γ_1, Γ^A, and κ). As the starting point, for the unbiased (V_g = 0 V) metasurface, we find that the fitting parameters should be set as $f_0 = f_1 = f_2 = 6.6$, $\Gamma_1 = \Gamma_2 = 0.54$, $\Gamma^A = 0$, $\kappa = -0.8$, $|d_{11}|^2 = |d_{22}|^2 = 1.07$, $|d_{12}|^2 = |d_{21}|^2 = 0.01$, all in units of GHz. The transmission/reflection/absorption spectra computed via Equations (3) and (4) with above fitting parameters are plotted in Figure 2c,h, which are in excellent agreement with both simulation and experimental results.

To reveal the underlying physics more clearly, we rewrite the transmission/reflection coefficients (t and r) and the absorption (A) of our system as the following independent-oscillator forms

$$\begin{aligned} &t = t_+ + t_- \text{ with } t_j = j\sqrt{\tilde{\Gamma}_j^S}\,\tilde{a}_j \\ &r = -1 + r_+ + r_- \text{ with } r_j = \sqrt{\tilde{\Gamma}_j^S}\,\tilde{a}_j \\ &A = A_+ + A_- \text{ with } A_j = 2\Gamma^A\left|\tilde{a}_j\right|^2 \end{aligned} \tag{5}$$

where $\tilde{a}_j = \sqrt{\tilde{\Gamma}_j^S}/(i(f - \tilde{f}_j) + \tilde{\Gamma}_j^S + \Gamma^A)$ with j = + (–) denoting the collective mode with symmetric (antisymmetric) wave function (see Section SII in the Supporting information). Through carefully examining Equation (5), we find that Γ^A is the only parameter tuned by the external bias voltage V_g, which must play an important role in manipulating the EM response of our system. We retrieved the $\Gamma^A \sim V_g$ relation (see Figure 3b) by fitting the CMT spectra with the FDTD ones (see dashed curves in Figure 2c–l and see CMT fitting parameters in Section SV in the Supporting Information). Obviously, Γ^A is an increasing function of V_g since increasing V_g decreases the inserted resistance of PIN diodes and thus enhances the absorptive decay rate of the resonator. Such $\Gamma^A \sim V_g$ dependence is also proven by the semi-analytical model shown in Figure S7c of Section IV in the Supporting Information. By inserting $\Gamma^A \sim V_g$ relation at the working frequency (f_0) into Equation (5), we obtain the $t_j(f_0) \sim V_g$, $r_j(f_0) \sim V_g$ and $A_j(f_0) \sim V_g$ relations as shown in Figure 3c–e. To better illustrate the physics, we plot in Figure 3c,d how the complex transmission and reflection coefficients vary as changing V_g in the complex plane (i.e., the Smith curves). We find that the transmission of our system decreases against Γ^A monotonically, but the absorption shows a nonmonotonic dependence on V_g, which reaches a maximum at a critical value $V_g = 0.55$ V.

We now establish a clear picture to understand the intriguing experimental behaviors reported in last section, based on our simplified model (Equation (5)). Obviously, the strengths of two collective modes (i.e., $\tilde{a}_j$) directly determine the transmitted signal since there is no background transmission (due to the presence of the metallic mesh) and re-emissions of these "modes" are the only sources to generate the transmitted signal. Enhancing the bias voltage V_g increases the intrinsic absorption inside the resonator, which, in turn, suppresses the mode amplitude $\tilde{a}_j$ (see Figure 3f). As the result, the transmission is naturally diminished, which exhibits a monotonic dependence on V_g. However, the same arguments do not apply to the absorption A of the system, since the absorption of a collective mode, $A_j = 2\Gamma^A\,|\,\tilde{a}_j\,|^2$, depends not only on the mode strength $\tilde{a}_j$ but also on the damping rate Γ^A. An interesting fact is that $\tilde{a}_j$ and Γ^A exhibit opposite dependences on V_g, and therefore, their competitions lead to a nonmonotonic V_g dependence of A. In particular, such intriguing competition dictates that the absorption can never reach 100%, but exhibits a maximum at a certain critical bias voltage.

The underlying physics is ultimately connected with the intrinsic correlations between transmission, reflection and absorption properties of systems exhibiting inversion symmetries. As clearly shown in Figure 3c,d, the inversion symmetry possessed by the system (with or without external bias voltage) impose the following strict constraints on the re-radiations of two collective modes to two different ports: $r_+ = t_+$ and $r_- = -t_-$. It is such symmetry-protected property that links the transmission coefficient t with the reflection coefficient r. In particular, although increasing V_g can decrease t through diminishing two scattering amplitudes t_+ and t_- (see Figure 3c), it also suppresses the strengths of r_+ and r_-, which results in enhanced reflection ($r = -1 + r_+ + r_-$, see Figure 3d). Such opposite V_g-dependences of $|t|$ and $|r|$ are the key reason accounting for the nonmonotonic V_g-dependence of the absorption A.

4. General Phase Diagram for Trilayer Tunable Metasurface

In last section, we already see that the inversion symmetry possessed by the metasurface imposes strict constrains on transmission and absorption properties of the system. Therefore, in order to realize full-range and independent manipulations on the transmission and absorption properties of a given system, we have to break the inversion symmetry of the system. Here, we keep using the symmetric ABA system as our basic structure, since it exhibits perfect transparency without external control. However, we choose to impose different voltages ($V_{g,1} \neq V_{g,2}$) on the PIN diodes loaded in two different A layers (see **Figure 4**a), which leads to different damping rates $\Gamma_1^A \neq \Gamma_2^A$ in our CMT model. Under such a biasing condition, we find that the evolutions of the symmetric and antisymmetric mode amplitudes $\tilde{a}_\pm$ are governed by

$$\frac{1}{2\pi}\frac{d}{dt}\begin{pmatrix}\tilde{a}_-\\ \tilde{a}_+\end{pmatrix} = \left[i\begin{pmatrix}\tilde{f}_- & 0\\ 0 & \tilde{f}_+\end{pmatrix} + \begin{pmatrix}-\tilde{\Gamma}_-^S & 0\\ 0 & -\tilde{\Gamma}_+^S\end{pmatrix} + \begin{pmatrix}-\tilde{\Gamma}_-^A & \tilde{X}_A\\ \tilde{X}_A & -\tilde{\Gamma}_+^A\end{pmatrix}\right]\begin{pmatrix}\tilde{a}_-\\ \tilde{a}_+\end{pmatrix} + \begin{pmatrix}\tilde{d}_{1-} & \tilde{d}_{2-}\\ \tilde{d}_{1+} & \tilde{d}_{2+}\end{pmatrix}\begin{pmatrix}S_1^{in}\\ S_2^{in}\end{pmatrix} \tag{6}$$

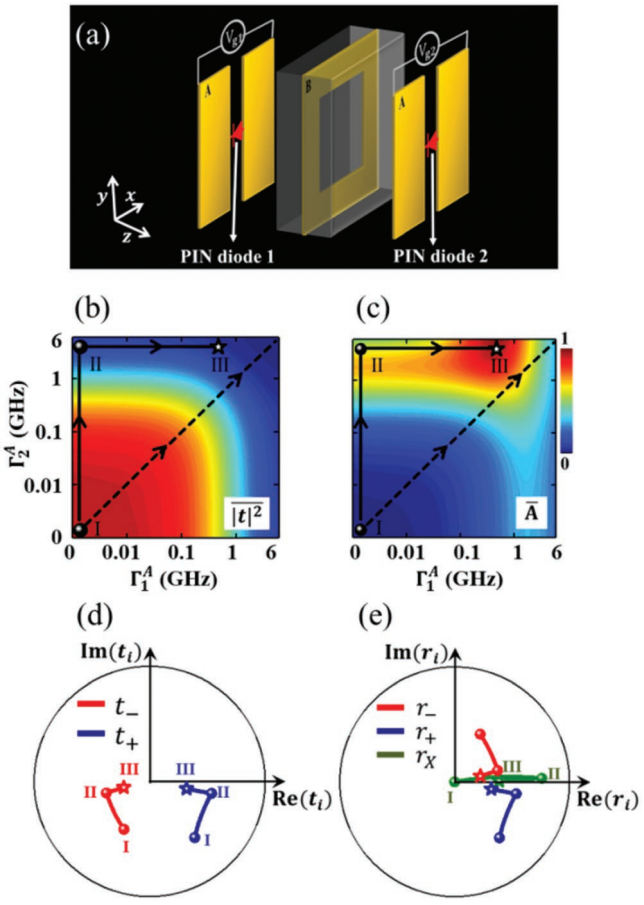

Figure 4. Geometry and working mechanism of our metasurface with applying bias voltages to two sides independently. a) Scheme of how the bias voltages are applied independently. Phase diagrams of b) transmission and c) absorption vary against absorptive decay rates (Γ_1^A and Γ_2^A). d) Smith curves of t_+ and t_- along the solid line path of indicated in the phase diagram. e) Smith curves of r_+, r_-, and r_X along the solid line path of indicated in the phase diagram.

where $\tilde{\Gamma}_+^A = \tilde{\Gamma}_-^A = (\Gamma_1^A + \Gamma_2^A)/2$ are the absorptive decay rates of the two modes and $\tilde{X}_A = (\Gamma_1^A - \Gamma_2^A)/2$ is absorption cross-coupling between two modes, caused by the inserted asymmetry. Solving Equation (6), we obtain the following expressions for the transmission and reflection coefficients

$$t = \frac{\tilde{X}_A(\tilde{d}_{1-}\tilde{d}_{2+} + \tilde{d}_{1+}\tilde{d}_{2-}) + \tilde{W}_-\tilde{\Gamma}_+^S - \tilde{W}_+\tilde{\Gamma}_-^S}{\tilde{W}_+\tilde{W}_- - \tilde{X}_A^2} = t_X + t_+ + t_- \tag{7}$$

$$r = -1 + \frac{2\tilde{X}_A\tilde{d}_{1-}\tilde{d}_{1+} + \tilde{W}_-\tilde{\Gamma}_+^S + \tilde{W}_+\tilde{\Gamma}_-^S}{\tilde{W}_+\tilde{W}_- - \tilde{X}_A^2} = -1 + r_X + r_+ + r_- \tag{8}$$

where $\tilde{W}_j = i(f - f_j) + \Gamma_j^S + \Gamma_j^A$, $t_+ = r_+ = \tilde{W}_-\Gamma_+^S/(\tilde{W}_+\tilde{W}_- - \tilde{X}_A^2)$, $t_- = -r_- = -\tilde{W}_+\Gamma_-^S/(\tilde{W}_+\tilde{W}_- - \tilde{X}_A^2)$. It is worth noting that t_j and r_j take different forms as those in Equation (5) due to the appearance of the cross-coupling damping rate $\tilde{X}_A$, although they possess similar physical meanings as those defined in Equation (5). Meanwhile, two new terms appear in such asymmetric cases, which are $r_X = 2\tilde{X}_A\tilde{d}_{1-}\tilde{d}_{1+}/(\tilde{W}_+\tilde{W}_- - \tilde{X}_A^2)$ and $t_X = \tilde{X}_A(\tilde{d}_{1-}\tilde{d}_{2+} + \tilde{d}_{1+}\tilde{d}_{2-})/(\tilde{W}_+\tilde{W}_- - \tilde{X}_A^2)$, denoting the cross-coupling terms in reflection and transmission coefficients, respectively. Considering further the symmetry properties of two collective modes ($\tilde{d}_{1+} = \tilde{d}_{2+}$ and $\tilde{d}_{1-} = -\tilde{d}_{2-}$), we find that t_X is strictly zero while r_X is not zero.

We now employ Equations (7) and (8) to compute how the transmission and absorption of our metasurface (calculated at the frequency $f_0 = 6.6$ GHz) vary against two damping parameters (Γ_1^A and Γ_2^A), and depict the obtained results in two phase diagrams shown in Figure 4b,c. Interestingly, we find that now the transmittance and absorption of our system can be independently controlled within full ranges via tuning two bias voltages (and thus Γ_1^A and Γ_2^A) appropriately. As shown in Figure 4b, perfect transmission occurs as $\Gamma_1^A, \Gamma_2^A \to 0$ (denoted as state I), while the transmittance decreases significantly as we increase either Γ_1^A or Γ_2^A (or both of them). Meanwhile, the absorption exhibits much more intriguing and richer behaviors. As shown in Figure 4c, perfect absorption ($A \approx 100\%$) only occurs inside a specific region with damping parameters satisfying $\Gamma_2^A \to 4$ GHz and $\Gamma_1^A \to 0.54$ GHz (denoted as state III), while the calculated absorption decreases significantly as leaving that region no matter one increases and decreases the damping rates. We note that perfect absorption can never happen along the line satisfying $\Gamma_1^A = \Gamma_2^A$, in consistency with our experimental results reported in last section for the symmetrically biased system. However, in present case with two bias voltages varying independently, we can choose any appropriate path connecting two states in the phase diagram to realize the functionality transition from perfect transparency (state I) to perfect absorption state (state III).

Without losing generality, we select one specific path to illustrate the underlying physics. We define an intermediate state as the state II (with $\Gamma_1^A = 0$ GHz and $\Gamma_2^A = 4$ GHz) to connect the states I and III through two straight lines (see the path defined in Figure 4b,c). With the $\Gamma^A \sim V_g$ relation known (see Figure 3b), we thus unambiguously know how the two bias voltages ($V_{g,1}$ and $V_{g,2}$) vary along the path. To make clear comparisons with the symmetric cases (Figure 3c,d), we purposely depict in Figure 4d,e as Smith curves how the complex amplitudes t_+, t_-, and r_+, r_- vary along the path defined in Figure 4b,c. It is not surprising to see that all Smith curves in Figure 4d,e contain two segments, which correspond to the evolutions of these complex amplitudes along the I–II path and the II–III path. Comparisons between Figures 4d,e and 3c,d reveal clearly the role played by the asymmetry-induced term r_X. Similar to the symmetric case, here in asymmetric case, we also find that the strength of $|r_+ + r_-|$ decreases along with the vanishing of $|t_+ + t_-|$. However, here we have an additional r_X to cancel the background reflection term -1 (see Equation (8)), which breaks the intrinsic correlation between t and r. As the result, through purposely adjusting this term, we can suppress both the transmission and reflection simultaneously to finally achieve perfect absorption under particular condition.

We now experimentally verify the above predications. As schematically depicted in Figure 4a, we apply different bias voltages on PIN diodes in two A layers following the requirement discussed above, and measure the transmittance/reflectance spectra of the metasurface. First, keeping $V_{g,1} = 0$ V, we increase $V_{g,2}$ continuously from 0 to 0.6 V, driving the system to transit from state I to state II. The measured transmittance spectra of

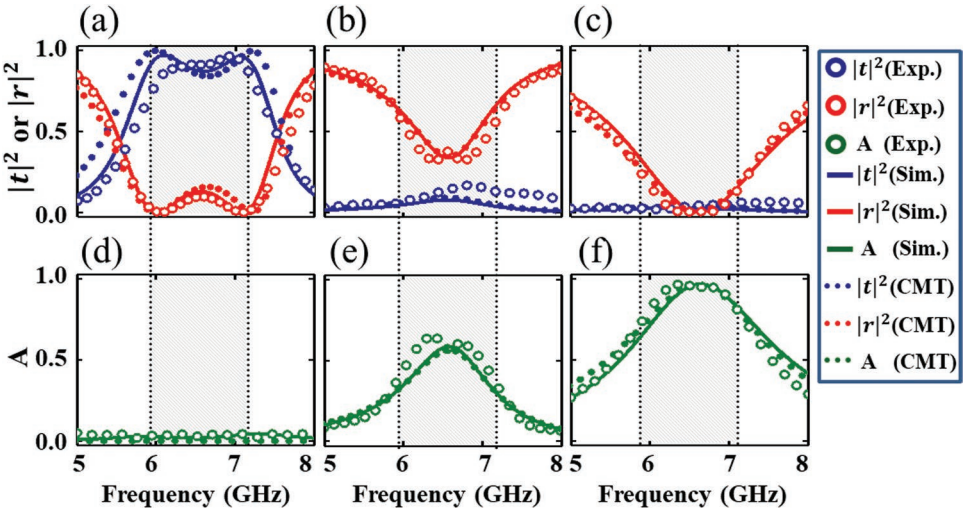

Figure 5. Simulated, measured and CMT results of the metasurface with applying bias voltages to two sides independently. a–c) The transmittance (blue), reflectance (red), and d–f) absorption (green), obtained by experiment (symbols), FDTD simulation (curves), and CMT mode (short dot).

our system are depicted in **Figure 5**a,b as blue lines. In consistency with our theoretical predictions, the peak transmittance of the system changes from nearly 100% to nearly 0 upon varying bias voltages along this line. Meanwhile, we note that the reflectance increases substantially and thus the total absorption does not reach 100% in state II, which is also consistent with the theoretical prediction. Next, we keep $V_{g,2}$ unchanged but increase $V_{g,1}$ from 0 to 0.53 V, which corresponds to the path from state II to state III as shown in Figure 4b,c. Measured transmittance/reflectance/absorption spectra of our system at the state III are depicted in Figure 5c,f, indicating clearly that the system (at this state) can indeed absorb EM waves completely suppressing both transmission and reflection, within the working frequency window. These results unambiguously demonstrated that we can switch the device's functionality from perfect transparency to perfect absorption with asymmetric biasing controls along the path defined in Figure 4b,c. Certainly, one can also choose other paths linking states I and III to achieve the desired functionality switching. Finally, we also performed FDTD simulations on the studied cases, and then retrieved the CMT parameters from the simulated spectra. The spectra obtained by FDTD simulations and the CMT model match very well with experimental results (Figure 5a–f).

5. Conclusion

To summarize, we employed the CMT to establish a general phase diagram for trilayer metasurfaces with loaded PIN diodes controlled asymmetrically, revealing the crucial role of inserted asymmetry from external controls in delinking the intrinsic connections between transmission and reflection properties of such ultrathin systems. Based on the phase diagram, we proposed an asymmetric biasing approach to realize a tunable transmissive metadevice with functionality switchable from perfect transparency to perfect absorption, and experimentally demonstrated the concept in the microwave regime. Our results can not only find immediate applications in practice, but also provide a new type of tunable meta-atoms for building tunable metadevices with dynamically controlled functionalities.

Supporting Information

Supporting Information is available from the Wiley Online Library or from the author.

Acknowledgements

Y.L. and J.L. contributed equally to this work. This work was supported by the National Key Research and Development Program of China (2017YFA0303500), the National Natural Science Foundation of China (11704240, 11734007, and 11674068), Natural Science Foundation of Shanghai (17ZR1409500 and 18QA1401800), Shanghai Science and Technology Committee (16JC1403100), Shanghai East Scholar Plan, and Fudan University-CIOMP Joint Fund.

Conflict of Interest

The authors declare no conflict of interest.

Keywords

coupled-mode theory, metamaterials, metasurfaces, perfect absorber, transparent window

Received: September 13, 2019
Revised: November 18, 2019
Published online: January 15, 2020

[1] L. Zhou, W. Wen, C. T. Chan, P. Sheng, *Phys. Rev. Lett.* **2005**, *94*, 243905.
[2] N. I. Landy, S. Sajuyigbe, J. J. Mock, D. R. Smith, W. J. Padilla, *Phys. Rev. Lett.* **2008**, *100*, 207402.

[3] N. Liu, M. Mesch, T. Weiss, M. Hentschel, H. Giessen, *Nano Lett.* **2010**, *10*, 2342.
[4] J. Hao, L. Zhou, M. Qiu, *Phys. Rev. B* **2011**, *83*, 165107.
[5] S. Li, S. Anwar, W. Lu, Z. H. Hang, B. Hou, M. Shen, C. H. Wang, *AIP Adv.* **2014**, *4*, 017130.
[6] N. Yu, P. Genevet, M. A. Kats, F. Aieta, J. P. Tetienne, F. Capasso, Z. Gaburro, *Science* **2011**, *334*, 333.
[7] S. Sun, Q. He, S. Xiao, Q. Xu, X. Li, L. Zhou, *Nat. Mater.* **2012**, *11*, 426.
[8] N. Yu, F. Capasso, *Nat. Mater.* **2014**, *13*, 139.
[9] H. T. Chen, A. J. Taylor, N. Yu, *Rep. Prog. Phys.* **2016**, *79*, 076401.
[10] S. Xiao, J. Wang, F. Liu, S. Zhang, X. Yin, J. Li, *Nanophotonics* **2016**, *6*, 215.
[11] Q. He, S. Sun, S. Xiao, L. Zhou, *Adv. Opt. Mater.* **2018**, *6*, 1800415.
[12] S. Sun, Q. He, J. Hao, S. Xiao, L. Zhou, *Adv. Opt. Photonics* **2019**, *11*, 380.
[13] F. Aieta, P. Genevet, N. Yu, M. A. Kats, Z. Gaburro, F. Capasso, *Nano Lett.* **2012**, *12*, 1702.
[14] X. Yin, Z. Ye, J. Rho, Y. Wang, X. Zhang, *Science* **2013**, *339*, 1405.
[15] S. Xiao, F. Zhong, H. Liu, S. Zhu, J. Li, *Nat. Commun.* **2015**, *6*, 8360.
[16] S. Wang, P. C. Wu, V. C. Su, Y. C. Lai, C. Hung Chu, J. W. Chen, S. H. Lu, J. Chen, B. Xu, C. H. Kuan, T. Li, S. Zhu, D. P. Tsai, *Nat. Commun.* **2017**, *8*, 187.
[17] C. Pfeiffer, A. Grbic, *Phys. Rev. Lett.* **2013**, *110*, 197401.
[18] S. Xiao, Q. He, X. Huang, S. Tang, L. Zhou, *Phys. Rev. B* **2012**, *85*, 085125.
[19] H. T. Chen, W. J. Padilla, J. M. Zide, A. C. Gossard, A. J. Taylor, R. D. Averitt, *Nature* **2006**, *444*, 597.
[20] B. Zhu, Y. Feng, J. Zhao, C. Huang, T. Jiang, *Appl. Phys. Lett.* **2010**, *97*, 051906.
[21] J. Zhao, Q. Cheng, J. Chen, M. Q. Qi, W. X. Jiang, T. J. Cui, *New J. Phys.* **2013**, *15*, 043049.
[22] Z. Miao, Q. Wu, X. Li, Q. He, K. Ding, Z. An, Y. Zhang, L. Zhou, *Phys. Rev. X* **2015**, *5*, 041027.
[23] H. X. Xu, S. Sun, S. Tang, S. Ma, Q. He, G. M. Wang, T. Cai, H. P. Li, L. Zhou, *Sci. Rep.* **2016**, *6*, 27503.
[24] Z. Tao, X. Wan, B. C. Pan, T. J. Cui, *Appl. Phys. Lett.* **2017**, *110*, 121901.
[25] K. Chen, Y. Feng, F. Monticone, J. Zhao, B. Zhu, T. Jiang, L. Zhang, Y. Kim, X. Ding, S. Zhang, A. Alù, C. W. Qiu, *Adv. Mater.* **2017**, *29*, 1606422.
[26] H. Yang, F. Yang, X. Cao, S. Xu, J. Gao, X. Chen, M. Li, T. Li, *IEEE Trans. Antennas Propag.* **2017**, *65*, 3024.
[27] L. Cong, P. Pitchappa, Y. Wu, L. Ke, C. Lee, N. Singh, H. Yang, R. Singh, *Adv. Opt. Mater.* **2017**, *5*, 1600716.
[28] L. Zhang, X. Q. Chen, S. Liu, Q. Zhang, J. Zhao, J. Y. Dai, G. D. Bai, X. Wan, Q. Cheng, G. Castaldi, V. Galdi, T. J. Cui, *Nat. Commun.* **2018**, *9*, 4334.
[29] Q. He, S. Sun, L. Zhou, *Research* **2019**, *2019*, 1849272.
[30] C. Qu, S. Ma, J. Hao, M. Qiu, X. Li, S. Xiao, Z. Miao, N. Dai, Q. He, S. Sun, Y. Zhang, L. Zhou, *Phys. Rev. Lett.* **2015**, *115*, 235503.
[31] S. Fan, W. Suh, J. D. Joannopoulos, *J. Opt. Soc. Am. A* **2003**, *20*, 569.
[32] H. Guo, J. Lin, M. Qiu, J. Tian, Q. Wang, Y. Li, S. Sun, Q. He, S. Xiao, L. Zhou, *J. Phys. D: Appl. Phys.* **2018**, *51*, 074001.
[33] B. Yang, T. Liu, H. Guo, S. Xiao, L. Zhou, *Sci. Bull.* **2019**, *64*, 823.
[34] W. Tan, Y. Sun, Z. G. Wang, H. Chen, *Appl. Phys. Lett.* **2014**, *104*, 091107.
[35] K. Chen, Y. Feng, L. Cui, J. Zhao, T. Jiang, B. Zhu, *Sci. Rep.* **2017**, *7*, 42802.
[36] We show in Supporting Information (Section SIII) that there is an intriguing interplay between absorption and transmission in such symmetric systems, and the maximum absorption achievable in such systems sensitively depends on the device's thickness. However, with any thicknesses, such tri-layer systems can never exhibit perfect transmission and perfect absorption through only varying the inserted absorption in PIN diodes. For the realistic metasurface studied here, the maximum absorption achievable is 66%.
[37] Cut-off frequency of the mesh is actually affected by the surrounding medium. Here, we have included the surrounding medium when we calculate the cut-off frequency of the mesh.
[38] B. Xi, H. Xu, S. Xiao, L. Zhou, *Phys. Rev. B* **2011**, *83*, 165115.